

## Seasonal nutrient and plankton dynamics in a physical-biological model of Crater Lake

Katja Fennel · Robert Collier · Gary Larson ·  
Greg Crawford · Emmanuel Boss

© Springer Science+Business Media B.V. 2007

**Abstract** A coupled 1D physical-biological model of Crater Lake is presented. The model simulates the seasonal evolution of two functional phytoplankton groups, total chlorophyll, and zooplankton in good quantitative agreement with observations from a 10-year monitoring study. During the stratified period in summer and early

fall the model displays a marked vertical structure: the phytoplankton biomass of the functional group 1, which represents diatoms and dinoflagellates, has its highest concentration in the upper 40 m; the phytoplankton biomass of group 2, which represents chlorophyta, chrysophyta, cryptomonads and cyanobacteria, has its highest concentrations between 50 and 80 m, and phytoplankton chlorophyll has its maximum at 120 m depth. A similar vertical structure is a reoccurring feature in the available data. In the model the key process allowing a vertical separation between biomass and chlorophyll is photoacclimation. Vertical light attenuation (i.e., water clarity) and the physiological ability of phytoplankton to increase their cellular chlorophyll-to-biomass ratio are ultimately determining the location of the chlorophyll maximum. The location of the particle maxima on the other hand is determined by the balance between growth and losses and occurs where growth and losses equal. The vertical particle flux simulated by our model agrees well with flux measurements from a sediment trap. This motivated us to revisit a previously published study by Dymond et al. (1996). Dymond et al. used a box model to estimate the vertical particle flux and found a discrepancy by a factor 2.5–10 between their model-derived flux and measured fluxes from a sediment trap. Their box model neglected the exchange flux of dissolved and suspended organic matter, which, as our model and available data suggests is significant for the

---

Guest Editors: Gary L. Larson, Robert Collier, and Mark W. Buktenica  
Long-term Limnological Research and Monitoring at  
Crater Lake, Oregon

---

K. Fennel (✉)  
Institute of Marine and Coastal Sciences and  
Department of Geological Science, Rutgers  
University, New Brunswick 08901, New Jersey, USA  
e-mail: kfennel@marine.rutgers.edu

R. Collier  
College of Oceanic and Atmospheric Sciences,  
Oregon State University, Corvallis 97331, Oregon,  
USA

G. Larson  
USGS Forest and Rangeland Ecosystems Center,  
Forest Science Laboratory Oregon State University,  
Corvallis 97331, Oregon, USA

G. Crawford  
Department of Oceanography, Humboldt State  
University, Arcata 95521, California, USA

E. Boss  
School of Marine Sciences, University of Maine,  
Orono 04473, Maine, USA

vertical exchange of nitrogen. Adjustment of Dymond et al.'s assumptions to account for dissolved and suspended nitrogen yields a flux estimate that is consistent with sediment trap measurements and our model.

**Keywords** Physical-biological model · Deep chlorophyll maximum · Photoacclimation · Crater Lake

## Introduction

Crater Lake is an ultra-oligotrophic, isolated caldera lake in the Cascade Mountains, Oregon. With a maximum depth of 590 m it is the deepest lake in the US and one of the clearest bodies of water on Earth. Crater Lake is surrounded by steep caldera walls, has a very small watershed and only small inputs of allochthonous matter. Most of the water entering the lake is direct precipitation onto its surface, which makes up 78% of its watershed. The remainder enters as run off from the caldera walls and as hydrothermal influx from the bottom (Collier et al. 1991). Despite its great depth, Crater Lake is relatively well-mixed. The upper portion of the lake (upper 200 m) is homogenized twice a year in early winter and late spring by free convection and wind-mixing (McManus et al. 1993). Partial ventilation of the deep lake occurs during these mixing periods when the upper water column is nearly isothermal (McManus et al., 1993) and during sporadic deep-mixing events (Crawford & Collier, 1997). Independent estimates of the lake ventilation time agree that the lake is ventilated on timescales of 1 to 5 years (Simpson, 1970; McManus et al., 1993; Crawford & Collier, 1997). Depletion of inorganic nitrogen species in the upper 200 m of the lake in summer implies nitrogen-limitation of phytoplankton growth, although bioassays suggest co-limitation by trace metals (Lane & Goldmann, 1984). Concentrations of inorganic phosphorus and silicic acid are relatively high and nearly uniform throughout the water column (Larson et al., 1996a). Vertical mixing is the most important source of new nutrients for primary production in the euphotic zone (Dymond et al., 1996). Comparisons of upward nutrient fluxes based on

box-model considerations and measurements of vertical particle fluxes from sediment traps reveal large discrepancies, i.e. the particle flux falls short of balancing the estimated upwelled nitrogen (Dymond et al., 1996).

The populations of microorganisms show distinct vertical maxima during stratified conditions (McIntire et al., 1996; Larson et al., 1996b; Urbach et al., 2001). In July and August, diatoms and dinoflagellates reach their maximum biomass in the upper 20 m of the water column, isolated from below by a pronounced thermocline. Chlorophyta, chrysophyta and cryptophyta dominate below the thermocline with biomass maxima between 80 and 100 m (Fig. 1) coincident with the vertical maximum of primary production (McIntire et al., 1996). The chlorophyll concentration has a deep maximum at a depth of 120 m, separated from the phytoplankton biomass maximum by about 50 m (Fig. 2). The vertical separation of the maxima in phytoplankton biomass (in units of carbon or nitrogen) and chlorophyll is mainly due to photoacclimation (Fennel & Boss, 2003) which results in dramatic vertical changes in the chlorophyll to biomass ratio (Fig. 2) and implies that the chlorophyll concentration does not represent phytoplankton biomass.

We developed a coupled physical-biological model of Crater Lake that captures the processes thought to determine nutrient cycling and phytoplankton production at first-order in a simplified description of the food-web. We consider the simplicity as valuable since it allows us to keep the number of poorly known model parameters at a minimum, but can elucidate dependencies and regulating mechanisms not easily seen in the observations alone. The model allows us to test hypotheses about the factors determining spatial and temporal patterns in species distribution, chlorophyll concentration, and primary production in relation to physical circulation processes. Here we present results of a 1-year model simulation in comparison with measurements obtained during a 10-year monitoring study (Larson, this issue), integrating the available data in a biomass-based framework. We discuss factors leading to the observed vertical distribution of phytoplankton populations and compare model-simulated vertical fluxes with particle flux measurements

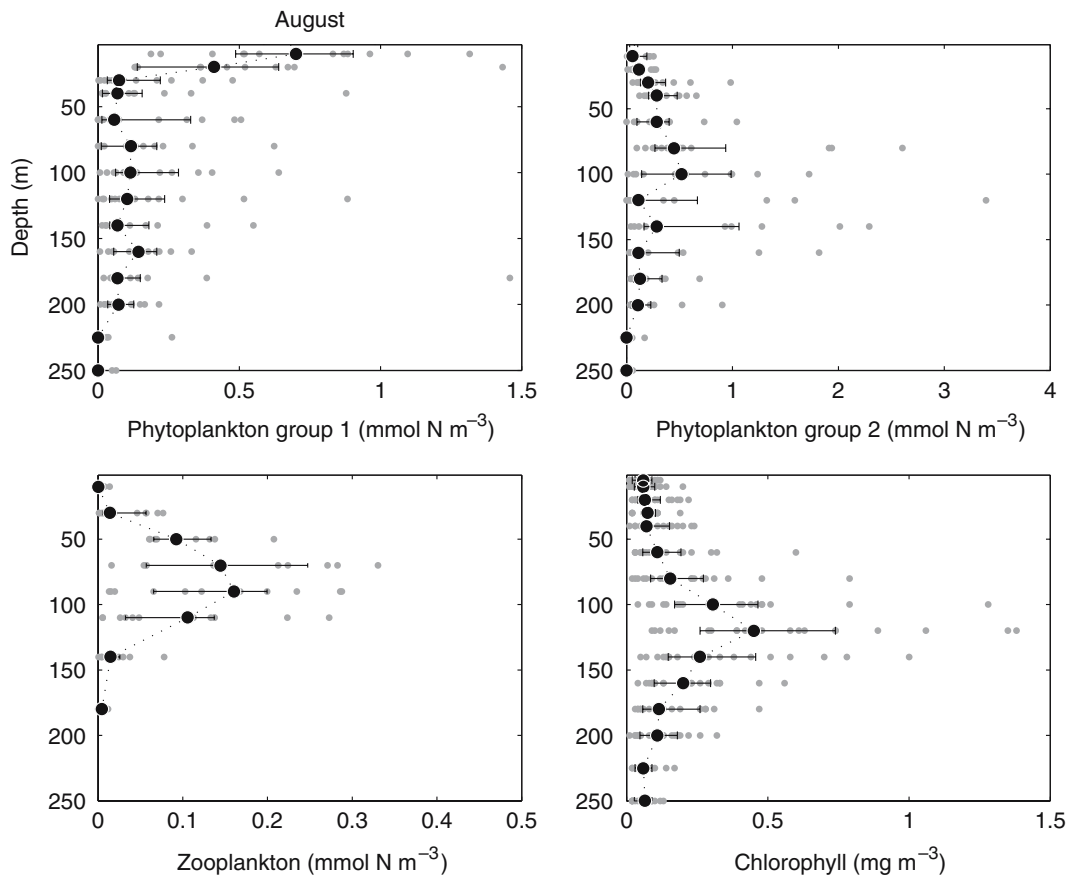


**Fig. 1** Available August data from 1989 to 2001 (gray bullets) and median with 25- and 75-percentiles (black bullets). Diatoms and dinoflagellates comprise phyto-

plankton group 1. Chlorophyta, chrysophyta, cryptomonads and cyanobacteria comprise phytoplankton group 2

and box-model estimates (Dymond et al., 1996) reconciling a previously reported mismatch.

## Materials & methods

### The biological model

We formulated a relatively simple biological model containing the following 7 state variables: dissolved nitrogen  $N$ , two phytoplankton groups  $P_1$  and  $P_2$ , one group of zooplankton  $Z$ , one detrital pool  $D$ , and the chlorophyll concentrations  $C_1$  and  $C_2$  of  $P_1$  and  $P_2$ , respectively (Fig. 3). All variables are expressed in units of  $\text{mmol N m}^{-3}$  except the chlorophyll variables, which are in  $\text{mg chl m}^{-3}$ . Nitrogen was chosen as the nutrient currency since Crater Lake is considered

nitrogen-limited (Lane & Goldman, 1984; Larsen et al., 1996a). Note that the nutrient variable  $N$  also includes dissolved organic nitrogen in addition to inorganic nitrogen. Technically detritus includes both, particulate and dissolved pools of organic nitrogen. However, the detritus variable  $D$  in our model is subject to vertical sinking. Hence, the dissolved organic nitrogen is more realistically treated as part of the nutrient pool  $N$ . The phytoplankton group  $P_1$  represents diatoms and dinoflagellates, i.e. the phytoplankton dominating in the upper 20 m of the water column.  $P_2$  comprises the remaining phytoplankton divisions (chlorophyta, chrysophyta, cryptomonads and cyanobacteria). The chlorophyll concentrations  $C_1$  and  $C_2$  of  $P_1$  and  $P_2$  are included as dynamical variables, to allow an explicit inclusion of photoacclimation.

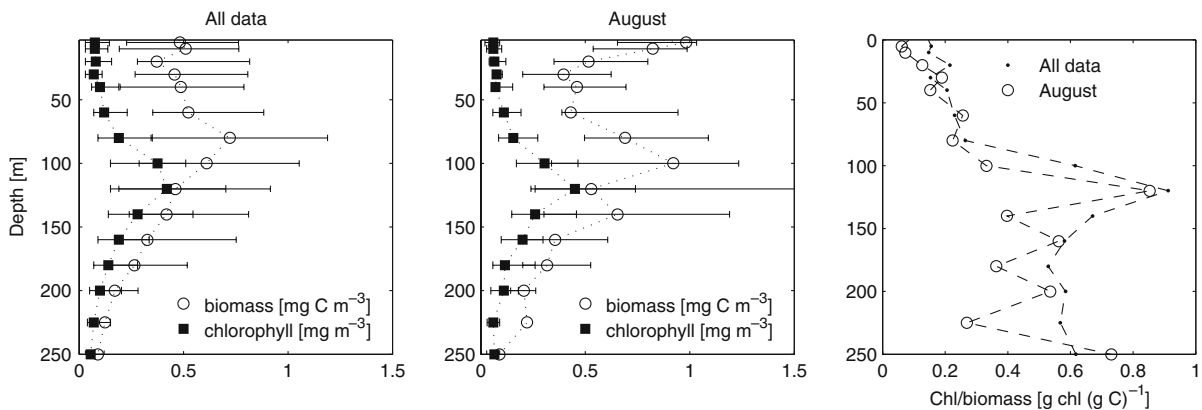


**Fig. 2** Median and 25- and 75-percentiles of chlorophyll and phytoplankton biomass. All data (left panel), August data (middle panel), and chlorophyll to biomass ratio (right panel) are shown

The dynamics of the biological state variables are determined by the following set of equations. The corresponding parameter values are given in Table 1. The biological sources minus sinks (sms) of the phytoplankton groups are defined as

$$sms(P_i) = \mu_i \cdot P_i - (L_{iN} + L_{iD}) \cdot P_i - g_i \cdot Z, \quad (1)$$

with  $i = 1, 2$ , where  $\mu_i$  is the phytoplankton growth rate,  $L_{iN}$  and  $L_{iD}$  are phytoplankton loss rates representing fluxes due to respiration and natural mortality, and  $g_i$  is the zooplankton grazing rate.

The phytoplankton growth rates  $\mu_i$  depend on the nutrient concentration  $N$ , following the Michaelis–Menten response, the photosynthetically available radiation  $E$  and the chlorophyll concentration  $C_i$  as

$$\mu_i^m = \mu_i^{\max} \left( 1 - \exp\left(-\frac{\alpha_i E C_i}{\mu_i^{\max} P_i}\right) \right), \quad (2)$$

$$\mu_i = \mu_i^m \frac{N}{k_{iN} + N} \text{ with } i = 1, 2. \quad (3)$$

Here  $\mu_i^{\max}$  is the maximum phytoplankton growth rate,  $\alpha_i$  is the chlorophyll-specific initial slope of the photosynthesis-irradiance curve, and  $k_{iN}$  is the half-saturation concentration for nutrient uptake. Note that we assume a tight coupling of nutrient uptake, growth and photosynthesis.

$E$  represents the light that is available for photosynthesis, which is determined for a given depth as

$$E(z) = E_0 \cdot par \cdot \exp\{-z(k_W + k_{Chl}chl|_z)\}, \quad (4)$$

where  $z$  is the water depth,  $E_0$  is the incoming shortwave radiation just below the lake surface, and  $par$  is the fraction of this radiation that is active in photosynthesis and assumed to be equal to 43%.  $k_W = 0.04 \text{ m}^{-1}$  and  $k_{Chl} = 0.03 \text{ m}^{-1} (\text{mg chl m}^{-3})^{-1}$  are the light attenuation coefficients for water and chlorophyll, respectively.  $chl|_z$  is the

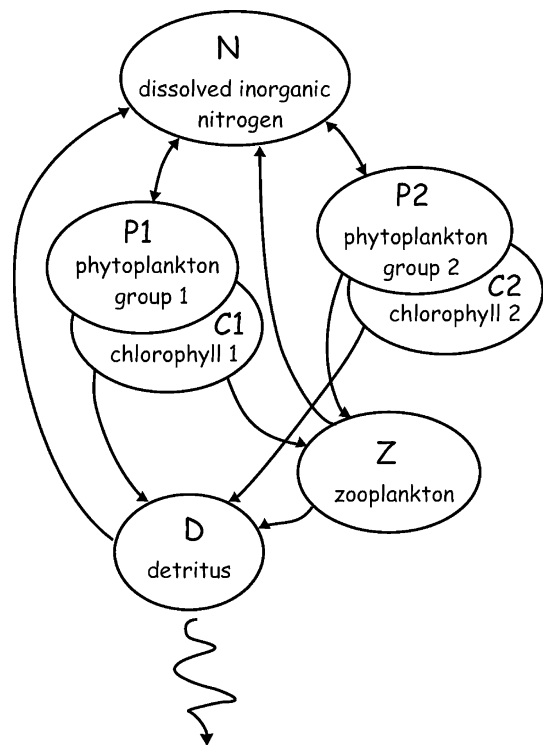


**Fig. 3** Schematic of the biological model component

**Table 1** Biological model parameters used in this study and range of published parameter values. N.D. denotes non-dimensional parameter

| Symbol            | Description  | Value | Unit   | Range                                     |
|-------------------|--|-------|--|---|
| $\mu_1^{\max}$    | maximum growth rate of $P_1$   | 1.50  | $\text{d}^{-1}$                                    | $0.62^{\text{a}}\text{--}3.0^{\text{b}}$  |
| $\mu_2^{\max}$    | maximum growth rate of $P_2$   | 0.85  | $\text{d}^{-1}$                                    | $0.62^{\text{a}}\text{--}3.0^{\text{b}}$  |
| $k_{1N}$          | half-saturation concentration for nutrient-uptake of $P_1$                         | 0.01  | $\text{mmol N m}^{-3}$                             | $0.0005\text{--}3.86^{\text{c}}$          |
| $k_{2N}$          | half-saturation concentration for nutrient-uptake of $P_2$                         | 0.01  | $\text{mmol N m}^{-3}$                             | $0.0005\text{--}3.86^{\text{c}}$          |
| $\alpha_1$        | chlorophyll-specific initial slope of the photosynthesis-irradiance curve of $P_1$ | 0.05  | $\text{mol N (g chl)}^{-1} (\text{W m}^{-2})^{-1}$ | $0.007\text{--}0.13^{\text{d}}$           |
| $\alpha_2$        | chlorophyll-specific initial slope of the photosynthesis-irradiance curve of $P_2$ | 0.7   | $\text{mol N (g chl)}^{-1} (\text{W m}^{-2})^{-1}$ | $0.007\text{--}0.13^{\text{d}}$           |
| $\Theta_1^{\max}$ | maximum ratio of chlorophyll to biomass of $P_1$                                   | 0.5   | $\text{g chl (mol N)}^{-1}$                        | maximum $5.6^{\text{e}}$                  |
| $\Theta_2^{\max}$ | maximum ratio of chlorophyll to biomass of $P_2$                                   | 6.0   | $\text{g chl (mol N)}^{-1}$                        | maximum $5.6^{\text{e}}$                  |
| $L_{1N}$          | loss rate from $P_1$ to $N$  | 0.13  | $\text{d}^{-1}$                                    | $0.02^{\text{i}}\text{--}0.1^{\text{g}}$  |
| $L_{1D}$          | loss rate from $P_1$ to $D$  | 0.06  | $\text{d}^{-1}$                                    | $0.05\text{--}0.2^{\text{f}}$             |
| $L_{2N}$          | loss rate from $P_2$ to $N$  | 0.15  | $\text{d}^{-1}$                                    | $0.02^{\text{i}}\text{--}0.1^{\text{g}}$  |
| $L_{2D}$          | loss rate from $P_2$ to $D$  | 0.15  | $\text{d}^{-1}$                                    | $0.05\text{--}0.2^{\text{f}}$             |
| $g_{\max}$        | maximum grazing rate   | 0.25  | $\text{d}^{-1}$                                    | $0.5^{\text{g}}\text{--}1.0^{\text{h}}$   |
| $K_3$             | half-saturation concentration for grazing  | 0.1   | $\text{mmol N m}^{-3}$                             | $0.75^{\text{i}}\text{--}1.89^{\text{j}}$ |
| $P_1$             | grazing preference for $P_1$   | 0.2   | N.D.   |   |
| $P_2$             | grazing preference for $P_2$   | 0.8   | N.D.   |   |
| $L_{ZN}$          | loss rate from $Z$ to $N$  | 0.1   | $\text{d}^{-1}$                                    | $0.04^{\text{g}}\text{--}15.0^{\text{j}}$ |
| $L_{ZD}$          | loss rate from $Z$ to $D$  | 0.1   | $\text{d}^{-1}$                                    | $0.04^{\text{g}}\text{--}15.0^{\text{j}}$ |
| $w_D$             | sinking rate of $D$  | 0.5   | $\text{m d}^{-1}$                                  | $0.009^{\text{k}}\text{--}10^{\text{l}}$  |
| $r$               | rem mineralization rate for $D$  | 0.3   | $\text{d}^{-1}$                                    | $0.05^{\text{k}}\text{--}0.18^{\text{m}}$ |

<sup>a</sup> Taylor, 1988<sup>b</sup> Anderson et al., 1987<sup>c</sup> Moloney & Field, 1991<sup>d</sup> Geider et al., 1997<sup>e</sup> Geider et al., 1998<sup>f</sup> Taylor et al., 1991<sup>g</sup> Wroblewski, 1989<sup>h</sup> Fasham, 1995<sup>i</sup> Palmer & Totterdell, 2001<sup>j</sup> Ross et al., 1994<sup>k</sup> Moskilde, 1996<sup>l</sup> Fasham, 1993<sup>m</sup> Jones & Henderson, 1986

mean chlorophyll concentration above the actual depth  $z$  and is determined by integrating over  $C_1$  and  $C_2$  as

$$\text{chl}|_z = \frac{1}{z} \int_0^z (C_1 + C_2) dz'. \quad (5)$$

The chlorophyll concentrations are determined following the photoacclimation model of Geider et al. (1996, 1997)

$$\text{sms}(C_i) = \rho_i \mu_i P_i - L_{iD} C_i - g_i Z \frac{C_i}{P_i}, \quad (6)$$

with

$$\rho_i = \Theta_i^{\max} \left( \frac{\mu_i P_i}{\alpha_i E C_i} \right). \quad (7)$$

$\Theta_i^{\max}$  is the maximum ratio of chlorophyll to biomass (in units of nitrogen) of phytoplankton group  $i$ .  $\rho_i$  represents the fraction of growth of phytoplankton  $i$  that is devoted to chlorophyll

synthesis and is regulated by the ratio of achieved-to-maximum potential photosynthesis  $(\mu_i P_i)/(\alpha_i EC_i)$  (Geider et al., 1997).

The zooplankton dynamics are determined by

$$sms(Z) = (g_1 + g_2)Z - (L_{ZN} + L_{ZD})Z, \quad (8)$$

$$g_i = g_{\max} \frac{p_i P_i}{k_3 + p_1 P_1 + p_2 P_2} \quad (9)$$

where  $i = 1, 2$ .  $g_{\max}$  is the maximum grazing rate,  $p_i$  are the grazing preferences (note that  $0 < p_1, p_2 < 1$  and  $p_1 + p_2 = 1$ ),  $k_3$  is the half-saturation concentration of grazing, and  $L_{ZN}$  and  $L_{ZD}$  are the zooplankton excretion and mortality rates.

The sources and sinks of the detrital pool are given by

$$sms(D) = L_{1D}P_1 + L_{2D}P_2 + L_{ZD}Z - rD - w_D \frac{\partial D}{\partial z}, \quad (10)$$

where  $r$  is the remineralization rate of detrital matter and  $w_D$  is the sinking rate.

The nutrient equation follows as

$$sms(N) = -\mu_1 P_1 - \mu_2 P_2 + L_{1N}P_1 + L_{2N}P_2 + L_{ZN}Z + rD. \quad (11)$$

### The physical model

The biological model is coupled to a one-dimensional physical model such that the evolution of any biological scalar  $X$  is given by

$$\frac{\partial X}{\partial t} = \frac{\partial}{\partial z} \left( k_z \frac{\partial X}{\partial z} \right) + sms(X), \quad (12)$$

where  $t$  is time and  $z$  is water depth. The first term on the right-hand side is the turbulent flux of  $X$ , and the second term represents the biological sources minus sinks of  $X$ , including the sinking of particles defined in the previous section. The physical model component is an implementation of the turbulent mixing scheme developed by Large et al. (1994) to simulate the planetary boundary layer in oceanic applications. Given surface fluxes of wind stress, heat and

freshwater, the model predicts the evolution of the surface boundary layer depth, the vertical eddy diffusivity profile  $k_z(z)$ , and the vertical profiles of temperature  $T$  and salinity  $S$ . The turbulent mixing of  $T$ ,  $S$  and biological scalars in the surface boundary layer is controlled by finite eddy diffusivities which decrease below the boundary layer. The boundary layer depth represents the penetration depth of surface-generated turbulence and does not resemble a surface mixed layer a priori.

### Model set up and forcing

The physical model is set up on an equidistant grid with 150 vertical levels of 4 m thickness. The model is forced with hourly values of the surface wind stress, the net shortwave radiation, the net longwave radiation, and sensible and latent heat fluxes. No evaporation or precipitation is included. Wind stress and heat fluxes were either measured directly or estimated from continuous measurements at one of the two meteorological stations located on a tower at the southwest caldera rim and on a buoy in the North Basin of the lake. The  $u$  and  $v$  components of the wind stress were determined from hourly averages of wind speed and direction. The net shortwave radiation was estimated from measurements of the downwelling shortwave radiation at the rim station and a parameterization of albedo following Payne (1972). The downwelling radiation at the rim was corrected to account for the shading effect of the caldera walls on the lake surface by a simple geometric argument. The net longwave heat flux is given by the downwelling longwave heat flux minus the longwave back radiation which was determined assuming the lake radiates like a grey body. The downwelling longwave heat flux was determined by a bulk parameterization depending on air temperature, water vapor pressure (determined from measurements of air temperature and relative humidity) and a cloudiness parameterization. The sensible heat flux was determined from the difference between the lake surface and air temperatures based on the bulk formula of Large & Pond (1982). The latent heat flux was determined from the evaporation rate following Large & Pond (1982).

Note that our model does not include the atmospheric precipitation of nitrogen and the nitrogen loss due to burial in the sediment and seepage. However, as the input from precipitation and the loss by burial and seepage balance (Dymond et al., 1996), this does not affect the overall nitrogen inventory of the lake. The initial conditions for the biological variables were obtained as follows: *N* was defined by interpolating the mean profile all available nitrate and ammonium data onto the model grid, while all other biological variables were set to 0.01 mmol N m<sup>-3</sup>. The model was then started on January 1 and run for 3 year to allow an adjustment to the initial conditions. All the results discussed here are from the third year of the simulation.

#### Limnological data

Water samples were collected from the RV Neuston at station 13 (42°56' N 122°06' W, located at the deepest part of Crater Lake) between June 1988 and September 2001. Nitrate and ammonia were measured by automated cadmium reduction and phenate calorimetric methods, respectively, and a Technicon autoanalyzer (Larson et al., 1996a). Chlorophyll concentrations were determined by fluorometry after filtration of samples onto 0.45- $\mu$ m pore-size filters and extraction with 90% acetone. Phytoplankton were preserved with Lugol's solution and concentrated by gravity settling (96 h). Cells > 1  $\mu$ m were identified and counted by means of inverted microscopy. Biovolume conversion factors were determined for each taxon by geometric approximation (McIntire et al., 1996). We converted biovolume to biomass (in units of carbon) by applying the following formula: cell C = 0.142 volume<sup>0.996</sup> [pg C  $\mu$ m<sup>-3</sup>] for each taxon. The conversion formula has been obtained by Rocha & Duncan (1985) by fitting 47 determinations of cell carbon and cell volume for 25 freshwater algal species.

Zooplankton samples were obtained by vertical towing of a 64- $\mu$ m mesh-size tow net. Zooplankton were diluted with pre-filtered lake water, preserved with 4% formaldehyde/4% sucrose, concentrated by gravity settling (24 h), and counted by means of inverted microscopy (Larson

et al., 1996b). Zooplankton weight conversion factors were estimated for each taxon from dried animals and used to convert organism densities to dry weight biomass (Larson et al., 1993). Here we converted from dry weight to biomass in units of carbon and nitrogen assuming that carbon constituted 48% and nitrogen 10% of dry weight respectively (Andersen & Hessen 1991; Brett et al., 2000).

#### Results

We present model results of a simulation for 1995 in comparison with observations. The simulated annual evolution of vertical distributions of the phytoplankton groups, total chlorophyll and zooplankton are shown in Fig. 4. Quantitative comparisons of the simulated concentrations with mean observations are given in Figs. 5–7.

The simulated total phytoplankton biomass is low from January through March. The biomass of phytoplankton group 2 (comprised of chlorophyta, chrysophyta, cryptomonads and cyanobacteria) starts to increase in April with increasing solar radiation before the upper water column stratifies thermally. Phytoplankton group 1 (diatoms and dinoflagellates) does not increase until thermal stratification is established in late May/early June (Fig. 4). During the stratified period in summer and early fall a marked vertical structure persists. The phytoplankton groups 1 and 2 express pronounced vertical maxima in the upper 40 m, and between 50 and 80 m, respectively (Figs. 4, 5). The low biomass in January and the vertical distribution of  $P_1$  and  $P_2$  compare well with the observed biomass of the “surface” and “deep” groups (Fig. 5). In particular, the profiles of phytoplankton group 2 agree remarkably well with the observed mean profiles of the “deep group” from June through September. The simulated vertical structure of phytoplankton group 1 agrees qualitatively with mean profiles of the “shallow group,” but the absolute surface concentrations are overestimated by our model in June and July.

The simulated chlorophyll profiles have a vertical maximum at about 120 m from June through August, about 50 m below the vertical maximum of phytoplankton group 2 (Figs. 4–6). The vertical

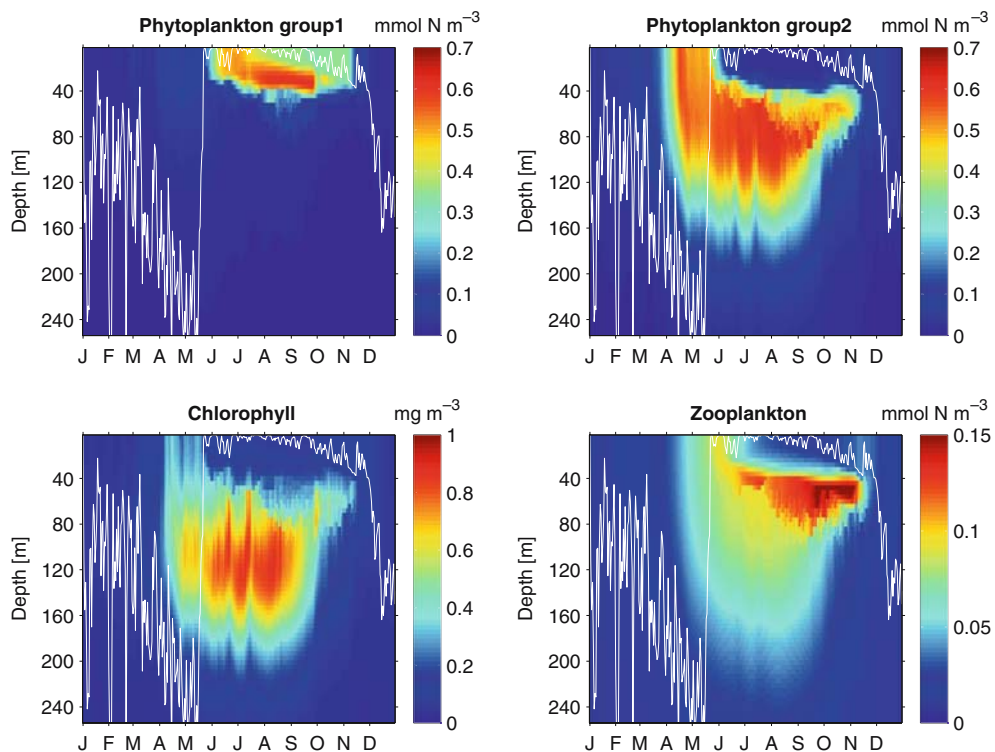


**Fig. 4** Simulated evolution of phytoplankton groups 1 and 2, total chlorophyll and zooplankton concentrations in the upper 250 m of the water column. The white line represents the depth of the simulated surface boundary layer

distribution of the simulated chlorophyll concentrations, which are low at the surface and increase monotonically to the deep maximum, agrees well with mean profiles of extracted chlorophyll (Fig. 6), but the absolute chlorophyll values are overestimated by the model.

The zooplankton concentrations are highest between 40 and 80 m and increase over the course of the growing season (Fig. 4). The magnitude of zooplankton biomass compares well with observed values, but a discrepancy in the vertical structure is apparent (Fig. 7). Some zooplankton species in Crater Lake exhibit diel vertical migrations with displacements between 20 and 40 m (Larson et al. 1993, 1996b). This behavior is not easily accounted for in the model but may explain the apparent discrepancy in vertical structure between simulated and observed zooplankton.

In summary, the model captures essential features of the system. Quantitative discrepancies exist and may stem from unresolved and/or poorly quantified processes.

## Discussion

We now discuss the seasonal evolution of vertical mixing and thermal stratification and its implications for the distribution of nutrients and plankton (section Physical controls of nutrient and plankton dynamics); suggest biochemical and bio-optical factors that contribute to the vertical structure of phytoplankton during the stable period in summer and early fall (section Biological factors for the vertical distribution of biomass and chlorophyll); and discuss a nitrogen budget for the watercolumn of Crater Lake (section Nitrogen budget).

### Physical controls of nutrient and plankton dynamics

Vertical mixing exerts important controls on the biological system, i.e., it affects nutrient supply to the euphotic zone, phytoplankton spatial distributions and light levels received by the phytoplankton community. We briefly describe the

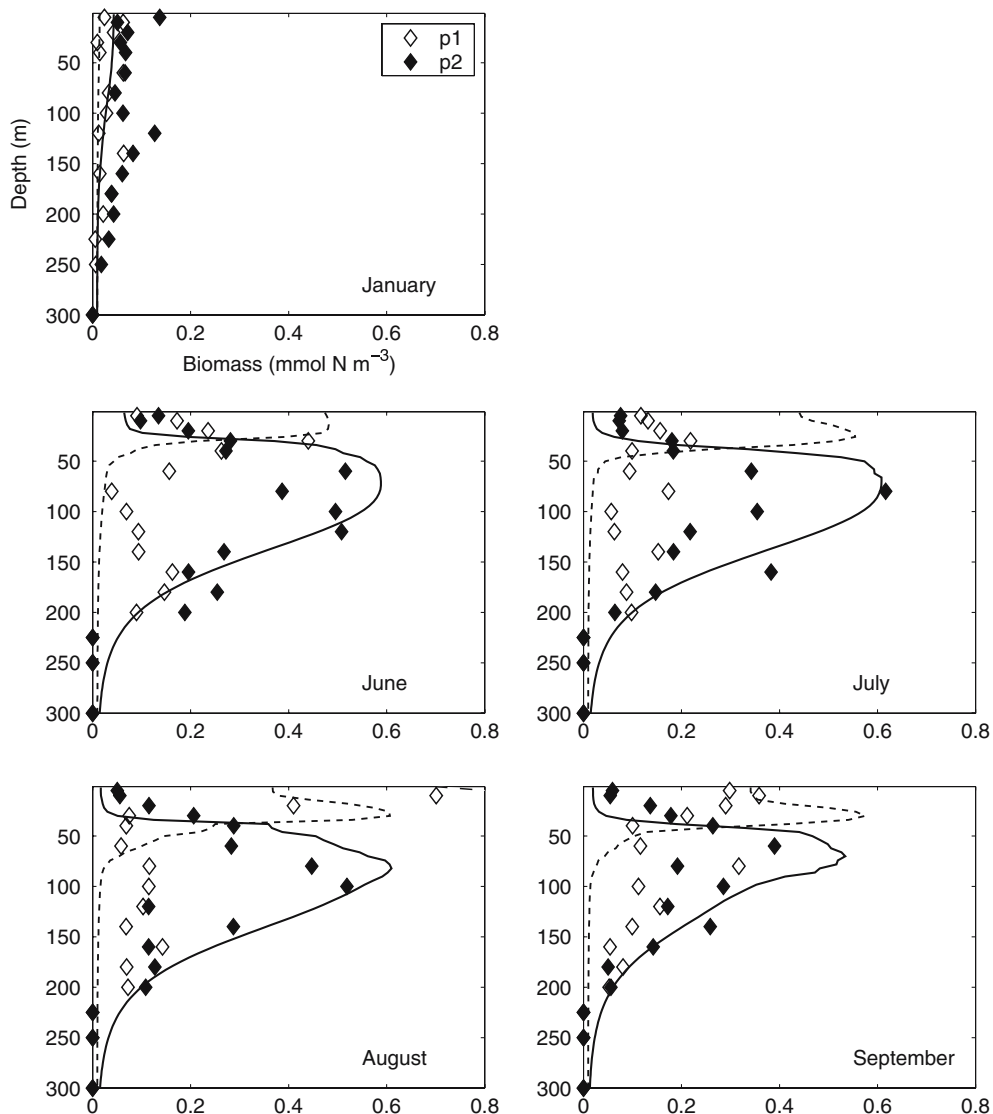


**Fig. 5** Simulated phytoplankton concentrations given as monthly means (solid and dashed lines) in comparison with medians of observed phytoplankton biomass (diamonds). P1 (open diamonds and solid lines) includes

diatoms and dinoflagellates. P2 (filled diamonds and dashed lines) includes chlorophyta, chrysophyta, cryptomonads and cyanobacteria

annual evolution of vertical mixing and stratification.

In winter and early spring the upper portion of Crater Lake (upper 200–250 m) is relatively well mixed. The water column is isothermal at two distinct events—once in early winter and once in early spring (McManus et al., 1993; Crawford & Collier 1997). The timing of these isothermal events and the intensity of mixing at a given time are determined by the current thermal structure and the surface wind stresses and heat fluxes. In

fall decreasing solar radiation and surface cooling erode the summer thermocline and produce cool, dense surface water that is convected. Convective mixing continues until the temperature of maximum density (about 4 °C) is reached. At this point the upper part of the water column is isothermal and a direct exchange of water between the upper and deep portions of the lake is possible. Continued cooling of surface water below the temperature of maximum density leads to inverse thermal stratification. Heating in early spring

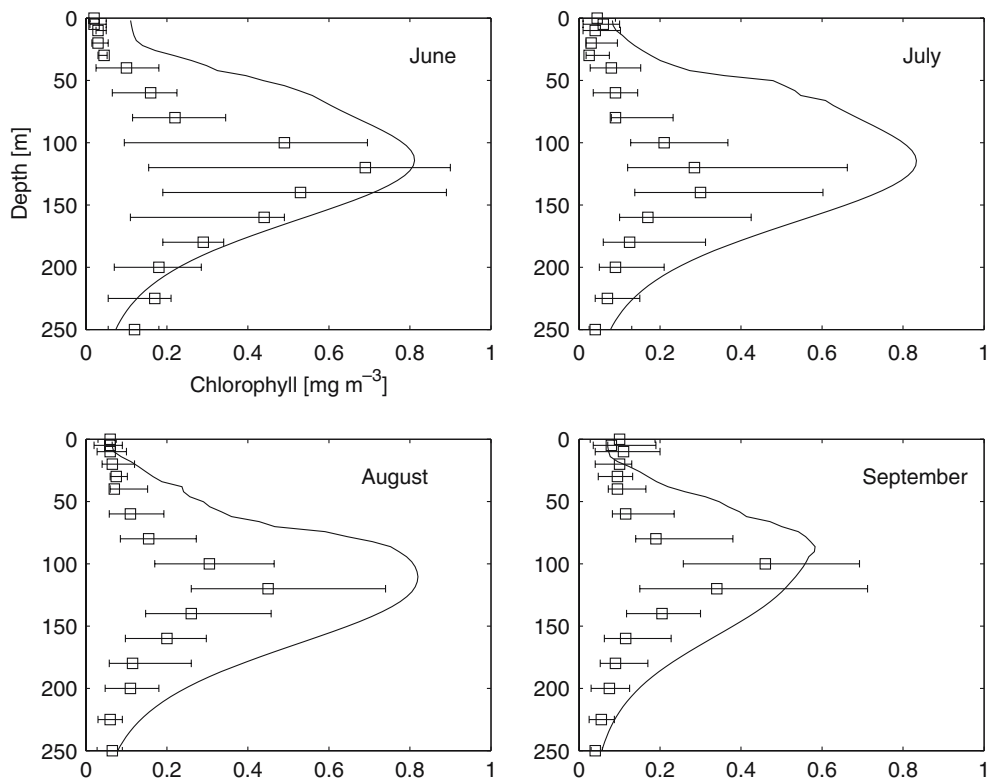


**Fig. 6** Simulated chlorophyll concentrations given as monthly means (solid lines) in comparison with observed chlorophyll data plotted as median with 25- and 75-percentiles (squares)

results in convective mixing until the temperature of maximum density is reached again—the second isothermal event. Subsequent heating leads to pronounced thermal stratification in summer. This evolution of convection and inverse thermal stratification is typical for high latitude systems below 20 PSU (e.g., Fennel, 1999; Botte & Kay, 2000).

The history of winter mixing affects processes in the euphotic zone in two important ways: (i) the most significant input of inorganic nutrients from the deep lake occurs during the isothermal periods (Dymond et al., 1996; Crawford & Collier, 1997); and (ii) as microorganisms are mixed vertically the photosynthetically active radiation (PAR) received by the phytoplankton community is strongly determined by mixing depth (Sverdrup, 1953). According to Sverdrup (1953) net phytoplankton growth in spring can only occur when the depth of vertical mixing is shallower than the critical depth (the depth at which the depth-integrated phytoplankton growth equals

depth-integrated respiration). In other words, net phytoplankton growth in spring can only occur in Crater Lake after the temperature of maximum density is exceeded and convective mixing ceases—a link that has been demonstrated for the spring bloom in the Baltic Sea (Fennel, 1999). Consistent with this concept phytoplankton biomass increases in our simulation only in April after the temperature of maximum density is exceeded in late March.

In summer a strong seasonal thermocline is established between 20 and 30 m depth and effectively limits vertical exchange. The vertical transport of nutrients is at a minimum and particles are not displaced vertically by advective forcings other than their own buoyancy forcing. The vertical transport of nitrate is restricted to turbulent diffusion. Since nitrate concentrations in the upper 100 m are low without a notable vertical gradient, a significant diffusive input to the euphotic zone can only occur below 100 m. Due to the stable stratification, microorganisms

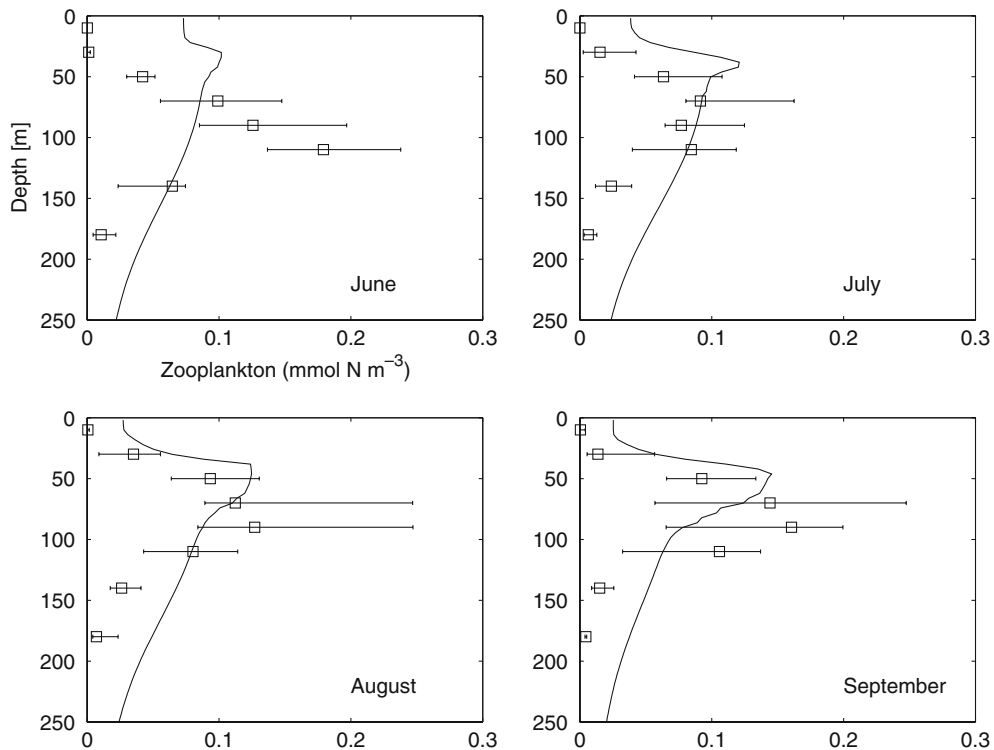


**Fig. 7** Stimulated zooplankton concentrations given as monthly means (solid lines) in comparison with observed zooplankton biomass plotted as median with 25- and 75-percentiles (squares)

can maintain their vertical position allowing for the observed and simulated dominance of distinct species groups at different depths (McIntire et al., this issue: Fig. 5).

#### Biological factors for the vertical distribution of biomass and chlorophyll

Our model captures a separation between the vertical maxima of phytoplankton biomass and chlorophyll (by up to 50 m) and the vertical differentiation between the phytoplankton functional groups 1 and 2 in agreement with observations. General criteria that determine the vertical structure of phytoplankton biomass and chlorophyll in stable, oligotrophic environments were discussed recently in Fennel & Boss (2003). We suggested that the particle maximum and the chlorophyll maximum are generated by fundamentally different processes. Photoacclimation results in a deep chlorophyll maximum vertically separated from the biomass maximum. During

stable conditions in summer and early fall, this vertical separation is pronounced in Crater Lake. The inclusion of photoacclimation in our model results in a vertical separation similar to the one observed. The location of the chlorophyll maximum is ultimately determined by light attenuation and the physiological ability of phytoplankton to increase their cellular chlorophyll-to-biomass ratio. The particle maximum on the other hand, is determined by the balance between biomass growth and losses including respiration, grazing, mortality, and divergence in sinking velocity.

Under steady-state conditions the biomass maximum is located at the depth where growth and losses equal (Riley et al., 1949; Fennel & Boss, 2003). This criterion can be derived as follows. Assuming that growth, biological losses (due to respiration, mortality and grazing), sinking and vertical mixing are the main processes determining the distribution of phytoplankton, a general 1D phytoplankton equation can be written as

$$\frac{\partial P}{\partial t} + \frac{\partial(wP)}{\partial z} = (\mu - R)P + \frac{\partial}{\partial z} \left( k_z \frac{\partial P}{\partial z} \right). \quad (13)$$

Here  $P$  represents the phytoplankton biomass,  $w$  the phytoplankton settling velocity,  $\mu$  the growth rate,  $R$  the rate of biological losses including respiration, mortality and grazing, and  $k_z$  the eddy diffusion coefficient. We want to solve Eq. 13 for steady state conditions, in which case the first term can be neglected and the equation simplifies to

$$\frac{d(wP)}{dz} = (\mu - R)P + \frac{d}{dz} \left( k_z \frac{dP}{dz} \right). \quad (14)$$

The condition for the location of a vertical phytoplankton maximum  $P(z_{\max})$  then follows as

$$\left. \frac{\partial P}{\partial z} \right|_{z_{\max}} = 0 \quad (15)$$

$$\Rightarrow \left( \mu - R - \frac{dw}{dz} \right) + k_z \frac{d^2 P(z_{\max})}{dz^2} = 0. \quad (16)$$

Since the particle maximum is usually located in a region with low diffusivity we neglect the diffusive flux term in Eq. 16 and obtain

$$\mu - R - \frac{dw}{dz} = 0. \quad (17)$$

In other words, at the particle maximum the community growth rate  $\mu$  equals the sum of the biological losses  $R$  and the divergence of particles due to changes in the settling velocity. This criterion can be applied to the phytoplankton groups 1 and 2 to predict the location of their vertical maxima (Fig. 8).

In our model the growth and loss term profiles of both phytoplankton groups differ mainly due to different parameter choices for the initial slope of the PI-curve  $\alpha_{\text{chl}}$  and the maximum growth rate  $\mu_{\text{max}}$  (see Table 1), although grazing and respiratory losses differ as well. The higher maximum growth rate of group 1 results in an advantage at high light levels near the surface, while the larger initial slope of phytoplankton group 2 is advantageous at lower light levels deeper in the water column. Unfortunately, no data are available on the light-physiological parameters of the algae

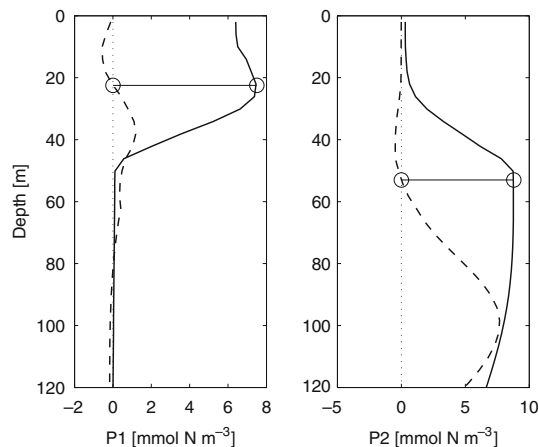


**Fig. 8** Mean July biomass of phytoplankton groups 1 and 2 (solid lines) and sum of their growth, respiration, grazing, mortality and diffusion terms on an arbitrary scale (dashed lines). The vertical biomass maxima occur where sources and sinks are equal as indicated by the circles

present in Crater Lake. Data from oceanic algae, however, are consistent with our parameter choices for  $\alpha_{\text{chl}}$  and  $\mu_{\text{max}}$ . Geider et al. (1997) collected photo-physiological parameters of 15 different marine algae from a wide range of environments (obtained from a total of 19 studies). We calculated the mean values of  $\mu_{\text{max}}$  and  $\alpha_{\text{chl}}$  for the 8 bacillariophyta and 11 chrysophyta included in this collection. The mean  $\mu_{\text{max}}$  equals  $3.6 \pm 1.3 \text{ d}^{-1}$  and  $1.3 \pm 0.9 \text{ d}^{-1}$  for bacillariophyta and chrysophyta, respectively, and the mean  $\alpha_{\text{chl}}$  equals  $0.05 \pm 0.36 \text{ mol N (g chl W m}^{-2}\text{)}^{-1}$  and  $0.054 \pm 0.34 \text{ mol N (g chl W m}^{-2}\text{)}^{-1}$  for bacillariophyta and chrysophyta, respectively. Consistent with our parameter choices the mean maximum growth rate is significantly higher for the bacillariophyta. There is no significant difference in  $\alpha_{\text{chl}}$  between both divisions, due to large variations between different taxa. Moore & Chisholm (1999) have shown that different isolates of *Prochlorochoccus* express distinct photo-physiological parameters. Comparing 10 different isolates they found two clusters: a high-light adapted group that had higher maximum light-saturated growth rates (corresponding to  $\mu_{\text{max}}$ ) and lower growth efficiencies under sub-saturating light intensities (corresponding to  $\alpha_{\text{chl}}$ ) than the low-light adapted group. These distinct ecotypes have been found to coexist in the same water column.

A potentially strong selective factor in the epilimnion in Crater Lake, not considered in our model is ultra-violet (UV) radiation. UV radiation is a significant stressor in aquatic environments. In Crater Lake, UV levels are particularly high. Incident UV radiation is elevated due to the high altitude and attenuation in the water column is small because concentrations of colored dissolved organic matter are low (Boss et al., this issue). Widely observed deleterious effects of UV on planktonic microorganisms include inhibition of photosynthesis (Lorenzen, 1979; Cullen et al., 1992; Smith et al., 1992) and bacterial heterotrophic potential (Herndl et al., 1993), and damage of DNA (Karentz et al., 1991). Two physiological acclimation mechanisms that decrease algal sensitivity to UV are efficient repair of photodamage, and the synthesis of photoprotective pigments (Litchman et al., 2002). In Crater Lake, the efficiency of both of these acclimation mechanisms is likely compromised by nitrogen limitation which has been observed to significantly depress the potential to repair photodamage and, to a lesser extent, the synthesis of photoprotective pigments (Litchman et al., 2002).

Despite the nitrogen limitation in Crater Lake, microorganisms in the epilimnion contain photoprotective pigments (Lisa Eisner, personal comm.). The usefulness of these pigments in decreasing sensitivity to UV radiation is strongly linked to organism size: for picoplankters (radii < 1  $\mu\text{m}$ ) pigment sunscreens are not of any relevance for photoprotection, but for microplankter (cell radii > 10  $\mu\text{m}$ ) these sunscreens can be very effective (Garcia-Pichel, 1994). Consequently, cell size represents a selective criterion, favoring larger cells in the epilimnion. This is consistent with optical measurements of the slope of the beam attenuation spectrum which point to the dominance of larger cells near the surface than at the deeper biomass maximum (Boss et al., this issue).

#### Nitrogen budget

The simulated sinking flux of detritus at 200 m in our model is 92  $\text{mg N m}^{-2} \text{yr}^{-1}$ . This value agrees well with vertical particulate nitrogen fluxes from

a sediment trap at 200 m measured between 1984 and 2002 (Dymond et al., 1996; Collier, R.W., unpublished data). The sediment trap data vary between 40 and 260  $\text{mg N m}^{-2} \text{yr}^{-1}$  with a mean of  $130 \pm 67 \text{ mg N m}^{-2} \text{yr}^{-1}$ . Note that our estimate is conservative as our model does not account for atmospheric inputs of nitrogen.

This agreement between simulated and observed fluxes stands in contrast to box-model estimates of vertical particle flux by Dymond et al. (1996), who found a significant discrepancy between estimated vertical particle fluxes and the sediment trap data. The authors derived an internal nitrogen budget, dividing Crater Lake into an upper and deep box (at 200 m) and formulating the nitrogen mass balance equations for both boxes as

$$F_p = F_a + F_r + F_u - F_d - F_{\text{sp,upper}} \quad (18)$$

and

$$F_p = \frac{1}{1 - \alpha} (F_u - F_d + F_{\text{sp,deep}}). \quad (19)$$

$F_p$  is the vertical flux of nitrogen due to settling particles.  $F_a$  and  $F_r$  are nitrogen sources to the upper box due to atmospheric inputs and runoff, respectively.  $F_u$  and  $F_d$  represent the nitrogen exchange between the upper and deep box due to upward mixing of deep-lake nutrients and downward mixing of surface nitrate pools, respectively.  $F_{\text{sp}}$  is the seepage loss of nitrogen through the lake floor, split into seepage losses from the upper and deep portions,  $F_{\text{sp,upper}}$  and  $F_{\text{sp,deep}}$ . The sediment burial term  $F_b$  is assumed to relate proportionally to the settling of particles  $F_p$  with  $\alpha$  representing the fraction of settling particles buried in the sediments ( $F_b = \alpha F_p$ ).

By inserting their best estimates of atmospheric, runoff and seepage inputs and losses, and a reasonable range of values for the burial fraction of settling particles into the right-hand-sides of Eqs. (18) and (19), Dymond et al. obtained model estimates for the vertical particle flux that were 2.5–10 times larger than the measured sediment trap fluxes. In their discussion the authors state that this discrepancy could be due to errors in the direct measurements, errors in their box-model assumptions, or unaccounted processes. They suggested a

combination of sediment focusing and significantly higher productivity at the edges of Crater Lake to explain the mismatch. Both of these processes are hard to quantify with the available data.

An analysis of our model results suggests a different explanation. We calculated the simulated exchange of nitrogen between the upper and deep box due to winter mixing as  $0.57 \times 10^6 \text{ mol yr}^{-1}$ . This value is significantly smaller than the flux assumed by Dymond et al. ( $2.0\text{--}4.0 \times 10^6 \text{ mol yr}^{-1}$ ). The authors obtained this exchange flux of nitrogen between the upper and deep boxes assuming (i) that winter mixing replaces  $2\text{--}4 \times 10^{12}$  liters of water between both boxes and (ii) a nitrate inventory of 0 and  $1 \mu\text{M}$  for the upper and deep boxes, respectively. They neglected the possibility of dissolved and suspended organic matter being exchanged between the upper and deep portions in addition to the exchange of nitrate. A flux of organic dissolved and suspended nitrogen could counterbalance an exchange of inorganic nitrogen. Interestingly, the simulated exchange of DIN in our model equals  $1.13 \times 10^6 \text{ mol yr}^{-1}$ , a value closer to Dymond et al.'s estimate, while the simulated exchange of organic matter is  $-0.56 \times 10^6 \text{ mol yr}^{-1}$ , reducing the net exchange to  $0.57 \times 10^6 \text{ mol yr}^{-1}$ .

In order to revisit the box-model calculations we estimate a “corrected” exchange flux ( $F_u - F_d$ ) based on the following arguments. Dymond et al. assumed a  $\Delta N$  (defined as the difference between nitrogen in the upper and deep portions of the lake) of  $1 \mu\text{M}$  neglecting dissolved and suspended nitrogen. We suggest a reduction of  $\Delta N$  to  $0.2 \mu\text{M}$ . We obtain this value assuming that the nitrate concentrations in the upper box equals 0 in agreement with Dymond et al., but reduce the assumed nitrate concentration in the deep box from 1 to  $0.6 \mu\text{M}$ . Our value is more representative of nitrate concentrations between 200 and 400 m depth—a water mass more likely to be mixed up above 200 m than water from below 400 m depth (Fig. 9). For estimates of dissolved and organic nitrogen we compare total Kjeldahl nitrogen (TKN) values between the upper and deep portions of the lake. TKN represents nitrogen in the ammonium, dissolved and particulate organic matter pools. TKN in the upper box is typically  $1.4 \mu\text{M}$  and TKN in the deep box is about  $1 \mu\text{M}$

(Fig. 9). With these nitrogen concentrations in the upper and deep boxes we obtain a  $\Delta N$  of  $0.2 \mu\text{M}$  and an exchange flux ( $F_u - F_d$ ) of  $0.4\text{--}0.8 \times 10^6 \text{ mol yr}^{-1}$ . This flux estimate compares well with our simulated flux of  $0.57 \times 10^6 \text{ mol yr}^{-1}$ . Iterating Dymond et al.'s box-model calculation with our estimate of  $F_u - F_d$ , we obtain vertical particle fluxes of  $0.69\text{--}1.38 \times 10^6 \text{ mol yr}^{-1}$  from Eq. (18) and  $0.5\text{--}1.1 \times 10^6 \text{ mol yr}^{-1}$  from Eq. (19). These revised box-model estimates are consistent with the sediment trap fluxes of  $0.49 \pm 0.25 \times 10^6 \text{ mol N yr}^{-1}$ , our model estimates, and the deep lake's oxygen budget (McManus et al., 1996).

## Conclusions

We developed a simple physical-biological model of Crater Lake that captures the observed vertical structure of two distinct phytoplankton groups and chlorophyll, and predicts the biomass of phytoplankton and zooplankton in good quantitative agreement with observations from a 10-year monitoring study. Our model suggests

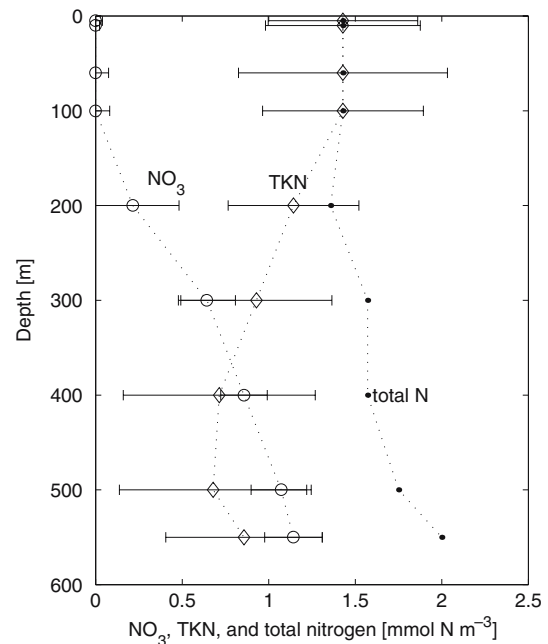


**Fig. 9** Mean profiles of nitrate and Kjeldahl nitrogen (represents the sum of ammonia, and particulate and dissolved nitrogen) with standard deviation, and total nitrogen

that phytoplankton production starts in spring only after the temperature of maximum density (about 4°C) is exceeded. That is, the onset of phytoplankton production is dependent on the evolution of vertical mixing in winter. Stable stratification in summer allows a pronounced vertical structure of phytoplankton distributions to emerge. The vertical separation of the deep chlorophyll maximum (at about 120 m) and the biomass maximum (between 50 and 80 m) results from photoacclimation. In our model the biomass maximum of both functional phytoplankton groups during stable conditions in summer is located where their respective growth and loss rates are equal. The differences in the vertical position of the biomass maximum of phytoplankton groups 1 and 2 at 20 m and 50–80 m, respectively, result mainly from parametric differences in the initial slope of the PI-curve and the maximum growth rate. While no experimental data on the growth and light-response parameters are available for the specific species present in Crater Lake, parameters determined for oceanic species are consistent with our choices. Sensitivity to UV radiation is likely to be an important selective factor as well, but is not included in our model since quantitative information on its effect is lacking. The average annual vertical flux of particles in our model compares well with the average annual flux measured in sediment traps at a depth of 200 m. We suggest correcting previous model estimates of vertical exchange by Dymond et al. (1996), who found a mismatch between model-estimated and observed vertical fluxes. Our model simulation pointed to a significant downward flux of suspended and dissolved organic matter which had been neglected by Dymond et al. Inclusion of this flux reconciles the box-model estimates and the trap measurements.

**Acknowledgements** We wish to thank Leon Tovey for reviewing the manuscript and three anonymous reviewers for helpful comments. Funding for KF was provided by USGS.

## References

- Andersen, T. & D. O. Hessen, 1991. Carbon, nitrogen and phosphorus content of freshwater zooplankton. *Limnology and Oceanography* 36: 807–814.
- Andersen, V., P. Nival & R. Harris, 1987. Modelling of a planktonic ecosystem in an enclosed water column. *Journal of the Marine Biological Association of the U.K.* 67: 407–430.
- Boss, E., R. Collier, G. Larson, K. Fennel & W. S. Pegau, this issue. Measurements of spectral optical properties and their relation to biogeochemical variables and processes in Crater Lake.
- Botte, V. & A. Kay, 2000. A numerical study of plankton population dynamics in a deep lake during the passage of the spring thermal bar. *Journal of Marine Systems* 26: 367–386.
- Brett, M. T., D. C. Mueller-Navarra & S.-K. Park, 2000. Empirical analysis of the effect of phosphorus limitation on algal food quality for freshwater zooplankton. *Limnology and Oceanography* 45: 1564–1575.
- Collier, R. W., J. Dymond & J. McManus, 1991. Studies of hydrothermal processes in Crater Lake, Oregon. *College of Oceanography Report*, 90. Oregon State University.
- Crawford, G. B. & R. W. Collier, 1997. Observations of a deep-mixing event in Crater Lake, Oregon. *Limnology and Oceanography* 42: 299–306.
- Cullen, J. J., P. J. Neale & M. P. Lesser, 1992. Biological weighting functions for the inhibition of phytoplankton photosynthesis by ultraviolet radiation. *Science* 258: 646–650.
- Dymond, J., R. Collier & J. McManus, 1996. Unbalanced particle flux budgets in Crater Lake, Oregon: Implications for edge effects and sediment focusing in lakes. *Limnology and Oceanography* 41: 732–743.
- Fasham M. J. R., 1993. Modelling marine biota. In Heimann M. (ed.), *The Global Carbon Cycle*. Springer Verlag, New York, 457–504.
- Fasham M. J. R., 1995. Variations in the seasonal cycle of biological production in subarctic oceans: A model sensitivity analysis. *Deep-Sea Research I* 42: 1111–1149.
- Fennel K., 1999. Convection and the timing of the phytoplankton spring bloom in the Western Baltic Sea. *Estuarine, Coastal and Shelf Sciences* 49: 113–128.
- Fennel K. & E. Boss, 2003. Subsurface maxima of phytoplankton and chlorophyll: Steady state solutions from a simple model. *Limnology and Oceanography* 48: 1521–1534.
- Garcia-Pichel F., 1994. A model for internal self-shading in planktonic organisms and its implications for the usefulness of ultraviolet sunscreens. *Limnology and Oceanography* 39: 1704–1717.
- Geider R. J., H. L. McIntyre & T. M. Kana, 1996. A dynamic model of photoadaptation in phytoplankton. *Limnology and Oceanography* 41: 1–15.
- Geider R. J., H. L. McIntyre & T. M. Kana, 1997. Dynamic model of phytoplankton growth and acclimation: Responses of the balanced growth rate and the chlorophyll a:carbon ratio to light, nutrient-limitation and temperature. *Marine Ecology Progress Series* 148: 187–200.
- Geider R. J., H. L. McIntyre & T. M. Kana, 1998. A dynamic regulatory model of phytoplankton acclimation to light, nutrients and temperature. *Limnology and Oceanography* 43: 679–694.

- Herndl G. J., G. Müller-Niklas & J. Frick, 1993. Major role of ultraviolet-b in controlling bacterioplankton in the surface layer of the ocean. *Nature* 361: 717–719.
- Jones R. & E. W. Henderson, 1986. The dynamics of nutrient regeneration and simulation studies of the nutrient cycle. *Journal du Conseil* 43: 216–236.
- Karentz D., J. E. Cleaver & D. L. Mitchell, 1991. Cell survival characteristics and molecular responses of Antarctic phytoplankton to ultraviolet-B radiation. *Journal of Phycology* 27: 326–341.
- Lane J. L. & C. R. Goldman, 1984. Size-fractionation of natural phytoplankton communities in nutrient bioassay studies. *Hydrobiologia* 118: 219–223.
- Large W. G. & S. Pond, 1982. Sensible and latent heat flux measurements over the ocean. *Journal of Physical Oceanography* 12: 464–482.
- Large W. G., J. C. McWilliams & S. C. Doney, 1994. Oceanic vertical mixing: A review and a model with non-local boundary layer parameterization. *Reviews of Geophysics* 32: 363–403.
- Larson, G. L., this issue. Overview over the Crater Lake program.
- Larson, G. L., C. D. McIntire, R. E. Truitt, M. W. Buktenica & K. E. Thomas, 1993. Zooplankton assemblages in Crater Lake. US Department of the Interior. Report, NPS/PNROSU/NRTR-93/03.
- Larson, G. L., C. D. McIntire, M. Hurley & M. W. Buktenica, 1996a. Temperature, water chemistry, and optical properties of Crater Lake. *Lake and Reservoir Management* 12: 230–247.
- Larson, G. L., C. D. McIntire, R. E. Truitt, M. W. Buktenica & E. Karnaugh-Thomas, 1996b. Zooplankton assemblages in Crater Lake, Oregon, USA. *Lake and Reservoir Management* 12: 281–297.
- Litchman, E., P. J. Neale & A. T. Banaszak, 2002. Increased sensitivity to ultraviolet radiation in nitrogen-limited dinoflagellates: Photoprotection and repair. *Limnology and Oceanography* 47: 86–94.
- Lorenzen, C. J., 1979. Ultraviolet radiation and phytoplankton photosynthesis. *Limnology and Oceanography* 24: 1117–1124.
- McIntire, C. D., G. L. Larson, R. E. Truitt & M. K. Debacon, 1996. Taxonomic structure and productivity of phytoplankton assemblages in Crater Lake, Oregon. *Lake and Reservoir Management* 12: 259–280.
- McIntire, C. D., G. L. Larson & R. E. Truitt, this issue. Taxonomic composition and production dynamics of phytoplankton assemblages in Crater Lake, Oregon.
- McManus, J., R. W. Collier & J. Dymond, 1993. Mixing processes in Crater Lake, Oregon. *Journal of Geophysical Research* 98C: 18295–18307.
- McManus, J., R. Collier, J. Dymond, C. G. Wheat & G. Larson, 1996. Spatial and temporal distribution of dissolved oxygen in Crater Lake, Oregon. *Limnology and Oceanography* 41: 722–731.
- Moloney, C. L. & J. G. Field, 1991. The size-based dynamics of plankton food webs. I. A simulation of carbon and nitrogen flows. *Journal of Plankton Research* 13: 1003–1038.
- Moore, L. R. & S. W. Chisholm, 1999. Photophysiology of the marine cyanobacterium *Prochlorococcus*: Ecotypic differences among cultured isolates. *Limnology and Oceanography* 44: 628–638.
- Moskilde, E., 1996. Topics in Non-linear Dynamics: Application to Physics, Biology and Economic Systems. World Scientific Publishing Co., London, U.K.
- Palmer, J. R. & I. J. Totterdell, 2001. Production and export in a global ocean ecosystem model. *Deep-Sea Research I* 48: 1169–1198.
- Payne, R. E., 1972. Albedo at the sea surface. *Journal of Atmospheric Science* 29: 959–970.
- Riley, G. A., H. Stommel & D. F. Bumpus, 1949. Quantitative ecology of the plankton of the western North Atlantic. *Bulletin of the Bingham Oceanographic Collection* 12: 1–169.
- Rocha, O. & A. Duncan, 1985. The relationship between cell carbon and cell volume in freshwater algal species used in zooplankton studies. *Journal of Plankton Research* 7: 279–294.
- Ross, A. H., W. S. C. Gurney & M. R. Heath, 1994. A comparative study of the ecosystem in four fjords. *Limnology and Oceanography* 39: 318–343.
- Simpson, H. J., 1970. Tritium in Crater Lake, Oregon. *Journal of Geophysical Research* 75: 5195–5207.
- Smith, R. C., B. B. Prezelin, K. S. Baker, R. R. Bidigare, N. P. Boucher, T. Coley, D. Karentz, S. MacIntyre, H. A. Matlick, D. Menzies, M. Ondrusek, Z. Wan & K. J. Waters, 1992. Ozone depletion: Ultraviolet radiation and phytoplankton biology in Antarctic waters. *Science* 255: 952–959.
- Sverdrup, H. U., 1953. On the conditions for the vernal blooming of phytoplankton. *Journal du Conseil Permanent International pour l'exploration de la Mer* 18: 287–295.
- Taylor, A. H., 1988. Characteristic properties of models for the vertical distribution of phytoplankton under stratification. *Ecological Modelling* 40: 175–199.
- Taylor, A. H., A. J. Watson, M. Ainsworth, J. E. Robertson & D. R. Turner 1991. A modelling investigation of the role of phytoplankton in the balance of carbon at the surface of the North Atlantic. *Global Biogeochemical Cycles* 5: 151–171.
- Urbach, E., K. L. Vergin, L. Young, A. Morse, G. L. Larson & S. J. Giovannoni, 2001. Unusual bacterioplankton community structure in ultra-oligotrophic Crater Lake. *Limnology and Oceanography* 46: 557–572.
- Wroblewski, J. S., 1989. A model of the spring bloom in the North Atlantic and its impact on ocean optics. *Limnology and Oceanography* 34: 1563–1571.